AquaMILR: Mechanical intelligence simplifies control of undulatory robots in cluttered fluid environments

Tianyu Wang^{1,†}, Nishanth Mankame^{1,†}, Matthew Fernandez¹, Velin Kojouharov², and Daniel I. Goldman¹

Abstract—While undulatory swimming of elongate limbless robots has been extensively studied in open hydrodynamic environments, less research has been focused on limbless locomotion in complex, cluttered aquatic environments. Motivated by the concept of mechanical intelligence [1], where controls for obstacle navigation can be offloaded to passive body mechanics in terrestrial limbless locomotion, we hypothesize that principles of mechanical intelligence can be extended to cluttered hydrodynamic regimes. To test this, we developed an untethered limbless robot capable of undulatory swimming on water surfaces, utilizing a bilateral cable-driven mechanism inspired by organismal muscle actuation morphology to achieve programmable anisotropic body compliance. We demonstrated through robophysical experiments that, similar to terrestrial locomotion, an appropriate level of body compliance can facilitate emergent swim through complex hydrodynamic environments under pure open-loop control. Moreover, we found that swimming performance depends on undulation frequency, with effective locomotion achieved only within a specific frequency range. This contrasts with highly damped terrestrial regimes, where inertial effects can often be neglected. Further, to enhance performance and address the challenges posed by nondeterministic obstacle distributions, we incorporated computational intelligence by developing a real-time body compliance tuning controller based on cable tension feedback. This controller improves the robot's robustness and overall speed in heterogeneous hydrodynamic environments.

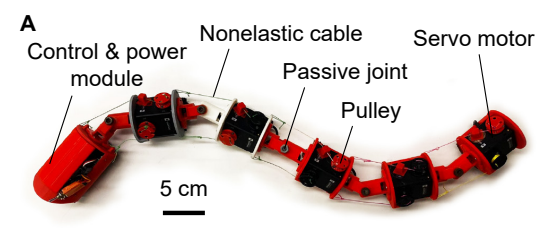
I. INTRODUCTION

Biologically inspired swimming robots have emerged as compelling candidates for navigating aquatic environments [2]–[8]. These robots offer versatile swimming modes and even enhanced speed and efficiency over conventional underwater vehicles in their application scenarios [9]-[13]. Specifically, elongate limbless (or snake-like, anguilliform) robots inspired by undulatory organisms, spanning from meter-scaled sea snakes and eels to millimeter-scaled nematodes, exhibit remarkable agility and maneuverability [4], [14]–[17]. This is due to their hyper-redundant body structure and ability to generate full-body undulation. However, despite extensive research in homogeneous hydrodynamic regimes, their locomotion in heterogeneous aquatic environments, particularly in highly cluttered scenarios where the body consistently interacts with multiple obstacles, remains less systematically studied.

 $^1\mathrm{Tianyu}$ Wang, Nishanth Mankame, Matthew Fernandez and Daniel I. Goldman are with Georgia Institute of Technology, Atlanta, Georgia, USA. tianyuwang@gatech.edu, nmankame3@gatech.edu, mfernandez64@gatech.edu, daniel.goldman@physics.gatech.edu

²Velin Kojouharov is now with Stanford University, Stanford, California, USA. vkojo@stanford.edu

†These authors contributed equally to this work.



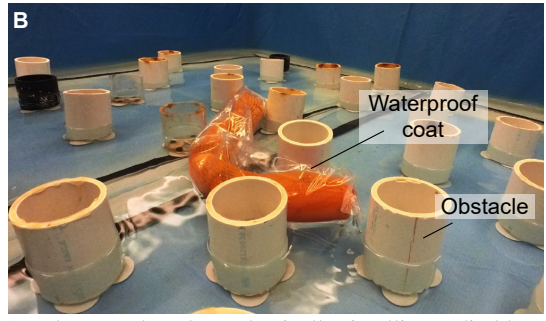


Fig. 1: The untethered mechanically intelligent limbless robot AquaMILR for undulatory locomotion in cluttered fluid environments. (A) The robot implements a decentralized bilateral actuation mechanism. (B) The robot navigates a laboratory model of an obstacle-rich environment.

Undulatory locomotion of limbless robots in homogeneous hydrodynamic environments has been studied for decades. Extensive research has demonstrated the efficacy and energy efficiency of this form of locomotion [14]-[16], [18]. By elucidating the principles underlying propulsion mechanisms, body morphology, and control strategies in controlled settings, these studies have significantly advanced our understanding of robotic undulatory swimming. However, in practical applications where challenges posed by environmental heterogeneities cannot be neglected, developing mechanisms to deal with obstacles becomes essential. Most existing systems employ perception-based obstacle-avoiding methods to prevent body-obstacle interactions [19], [20]. However, these approaches require large onboard computational power and/or high-quality communication and data transmission for off-board processing. More importantly, they become less effective in obstacle-rich regions where multiple interactions occur simultaneously along the body and cannot be avoided.

Although not widely applied to hydrodynamic scenarios, obstacle adaptation (or obstacle-aided) [21], [22] mechanisms offer another major approach for limbless robot locomotion in obstacle-rich terradynamic regimes, apart from the obstacle-avoiding approach. Unlike methods that rely heavily on sensing and environmental knowledge [23], [24], methods that realize body compliance through purely pas-

sive mechanics [1], [25]–[27] are particularly suited for aquatic applications, as they minimize the computation and communication required. Specifically, [1] developed a robot (Mechanically Intelligent Limbless Robot, MILR) that models the musculoskeletal actuation mechanisms of snakes and nematodes. By comparing the kinematics of biological and robotic locomotion, this study demonstrates that the robot can spontaneously navigate obstacles using a preprogrammed body compliance induced by a cable-actuated mechanism, without relying on active feedback control. We refer to this phenomenon—leveraging passive body mechanics to simplify control and enhance capabilities in complex terrains—as "mechanical intelligence."

Although programmable body compliance via bilateral cable actuation has been shown to facilitate emergent obstacle navigation in terrestrial settings, its applicability in aquatic environments remains uncertain. This work investigates whether this form of mechanical intelligence extends to hydrodynamic regimes, where inertial effects at intermediate Reynolds numbers introduce coasting behavior and fundamentally alter undulatory propulsion dynamics [28]–[31]. While swimming in open water is relatively straightforward to achieve, this study focuses instead on the challenges of navigating cluttered aquatic environments, where interactions with obstacles significantly impact locomotion. Our contributions are twofold: (1) we systematically analyze how varying levels of mechanical intelligence influence locomotion in hydrodynamic settings using a robophysical approach [32], and (2) we develop strategies for undulatory limbless robots to navigate complex, obstacle-dense environments by leveraging passive body mechanics. This study extends mechanical intelligence beyond terrestrial systems, informing the development of aquatic limbless robots.

II. UNTETHERED ROBOT DEVELOPMENT AND CONTROL

A. Robot design and manufacturing

To investigate principles of mechanical intelligence in heterogeneous aquatic environments, we developed a modular limbless robot based on the MILR design [1]. Our 66-cm-long hard-soft hybrid model features 5 bending joints (Fig. 1A) and employs a bilateral actuation mechanism. Passive bending joints are controlled by adjusting cable lengths via decentralized cable-pulley-motor systems, with each cable independently managed on either side of the joint. By synchronizing the cable lengths through sequential angular oscillations along the body, the robot generates undulatory motion.

In intermediate Reynolds numbers aquatic environments, locomotion is highly sensitive to inertial effects, where even small forces can disrupt overall performance. To minimize such perturbations, we employed an untethered design. Specifically, we designed a control and power module housed in the robot's head (Fig. 1A). This head module integrates a single-board computer, a motor communication converter, a voltage regulator, and a battery.

The entire robot body, including the casing, joint links, and pulleys, was 3D printed from PLA filament. For the

cable-pulley-motor systems, we controlled the lengthening and shortening of the nonelastic cables (Rikimaru Zero Stretch & Low Memory) with Dynamixel 2XL430-W250-T (Robotis) servo motors, which provide up to 1.4 Nm torque. To waterproof the system, a tube-shaped polyethylene plastic sleeve was used to encase the robot (Fig. 1B). The robot was placed inside a section of tubing, and the plastic was heat-sealed at both ends to create a watertight seal. This design allowed the robot to effectively swim on the surface of the water

The head module featured a removable top and housed a single-board computer (Raspberry Pi Zero 2W) for onboard computation, real-time communication with a PC via Wi-Fi, and real-time control of the servo motors through a Dynamixel U2D2. A 1000-mAh 3-cell LiPo battery powered all the motors and the single-board computer: the motors received 12V, while a 5V/2.5A voltage regulator stepped down the voltage for the computer.

We named the robot, following MILR as in [1], as AquaMILR, and it will be referenced as such throughout the remainder of this paper.

B. Suggested gait

To achieve a basic traveling-wave locomotion pattern on AquaMILR, we designed a shape control scheme based on the "serpenoid" shape template introduced by [33]. This template allows a wave to move from the head to the tail of the robot when the angle of the i-th joint angle, α_i , at time t is given by

$$\alpha_i(t) = A\sin(2\pi\xi \frac{i}{N} - 2\pi\omega t),\tag{1}$$

where A denotes the amplitude, ξ is the spatial frequency, ω is the temporal frequency, i is the joint index, and N is the total number of joints. This angle α_i is referred to as "suggested" angle.

To precisely achieve the joint angle α as defined in Eq. 1, it is necessary to adjust the lengths of the left and right cables around the joint, ensuring both are appropriately shortened (as shown in Fig. 2A). Note that we use nonelastic cables, their deformation is negligible. The lengths of the left cable (\mathcal{L}^l) and right cable (\mathcal{L}^r) are determined by the robot's geometry then, as illustrated in Fig. 2A, and follow these equations:

$$\mathcal{L}^{l}(\alpha) = 2\sqrt{L_{c}^{2} + L_{j}^{2}} \cos \left[-\frac{\alpha}{2} + \tan^{-1} \left(\frac{L_{c}}{L_{j}} \right) \right],$$

$$\mathcal{L}^{r}(\alpha) = 2\sqrt{L_{c}^{2} + L_{j}^{2}} \cos \left[\frac{\alpha}{2} + \tan^{-1} \left(\frac{L_{c}}{L_{j}} \right) \right],$$
(2)

where L_c is the distance between the cable anchoring point on the casing and the center of the casing, and L_j is the length of the joint.

C. Programmable body compliance

Using Eq. 2, we can accurately implement body postures for lateral undulation gaits in the robot. Further, the advantage of implementing the bilateral actuation mechanism is that it allows us to program body compliance by coordinately loosening the cables. By applying the generalized

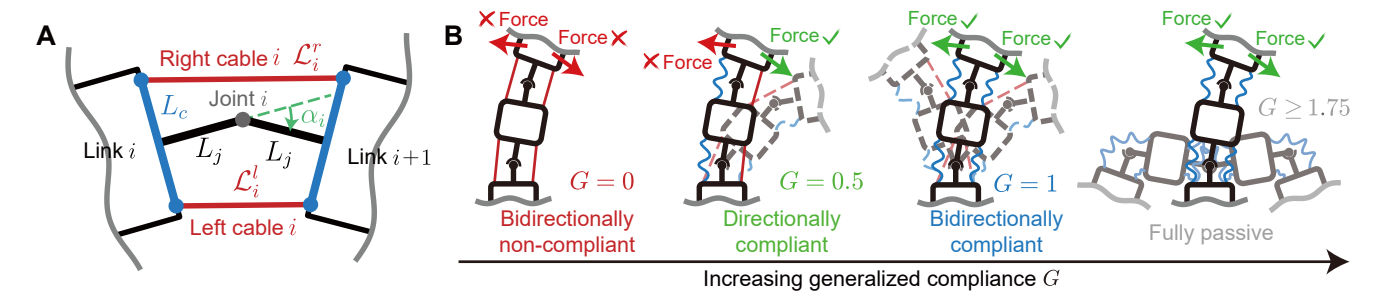


Fig. 2: Programmable and quantifiable body compliance through bilateral cable actuation mechanism. (A) A geometric model illustrating a single joint, used to determine the exact lengths of the left and right cables (\mathcal{L}^l and \mathcal{L}^r) necessary to achieve a specified joint angle (α). (B) A schematic displaying various compliance states based on the generalized compliance variable G: bidirectionally non-compliant (G = 0), directionally compliant (G = 0.5), bidirectionally compliant (G = 0.5), and fully passive ($G \ge 1.75$). Figures adapted from [1].

compliance variable (G) as defined in [1], we can quantify AquaMILR's body compliance. The cable length control scheme sets the lengths of each pair of left and right cables (L_i^l) and L_i^r based on the corresponding suggested angle (α_i) :

$$L_{i}^{l}(\alpha_{i}) = \begin{cases} \mathcal{L}_{i}^{l}(\alpha_{i}), & \text{if } \alpha_{i} \leq -\gamma \\ \mathcal{L}_{i}^{l}[-\min(A,\gamma)] + l_{0} \cdot [\gamma + \alpha_{i}], & \text{if } \alpha_{i} > -\gamma \end{cases}$$

$$L_{i}^{r}(\alpha_{i}) = \begin{cases} \mathcal{L}_{i}^{r}(\alpha_{i}), & \text{if } \alpha_{i} \geq \gamma \\ \mathcal{L}_{i}^{r}[\min(A,\gamma)] + l_{0} \cdot [\gamma - \alpha_{i}], & \text{if } \alpha_{i} < \gamma \end{cases}$$
(3)

where the superscripts l and r denote left and right, respectively, and $\gamma = (2G_i - 1)A$. The design parameter l_0 determines the relaxed length of a cable, which is fixed at 0.73 mm/° for this work (for a full discussion on choosing l_0 and its derivation, refer to [1]). Following Eq. 3, the robot can achieve three representative compliance states with varying G (Fig. 2B): 1) bidirectionally non-compliant (G = 0), where each joint angle strictly follows the suggested gait template in Eq. 1; 2) directionally compliant (G = 0.5), where the joints are only allowed to deviate to form a larger angle than suggested; and 3) bidirectionally compliant (G = 1), where the joints can deviate in both directions, regulated by Eq. 3. Note that $G \in [0, \infty)$ is a continuous value: for any value of G between the representative compliance states, the joint shows a hybrid compliance state based on the real-time suggested angle α ; when G exceeds 1 and keeps increasing, the joint remains bidirectional compliant and becomes more slack until it reaches a fully passive state (G = 1.75 in this work).

III. EXPERIMENT

A. Experiment setup

To create a laboratory aquatic environment for testing AquaMILR's performance, we set up an indoor pool with dimensions of 3 m \times 2 m \times 0.5 m ($L \times W \times H$) and a water level of 20 cm. Obstacles were constructed using 9 cm diameter PVC pipes, each equipped with suction cup feet at the bottom (Fig. 1B). These obstacles were arranged in a triangular grid pattern with 25 cm spacing (Fig. 3). In short, the triangular obstacle terrain will be referred to as the lattice throughout the rest of paper. The lattice measures 2 m \times 2 m. The suction cups ensured secure attachment of the obstacles to a plexiglass sheet, providing a stable and smooth surface that is submerged to the pool floor. Consequently, the obstacles in the heterogeneous aquatic terrain utilized

throughout this study maintained their shape and position without deformation or displacement upon collisions with AquaMILR.

B. Robophysical experiment

We conducted robophysical experiments to investigate how different parameters influenced the robot's ability to navigate the lattice. As a starting point, we selected $A=55^{\circ}$ and $\xi=0.6$ as our baseline gait based on previous work, ensuring that the robot's body wavelength-to-lattice spacing ratio matched that of the terrestrial case, where emergent passive obastacle navigation was previously demonstrated [1].

First, we examined the effect of body compliance. In this set of experiments, we maintained a consistent G value across all joints and varied it to observe performance differences. In terradynamic regimes, previous work experimentally determined that a G value between 0.75 and 1 provided appropriate compliance for maneuvering through various heterogeneous terrains [1]. To assess whether this principle applies to aquatic settings, we tested G values ranging from 0 to 1.5 in increments of 0.25.

Next, we explored the effects of spatial frequency and amplitude on locomotion, as defined in Eq. 1. For spatial frequency tests, we examined values ranging from 0.3 to 1.2 in increments of 0.3, omitting higher values due to the robot's limited length, while maintaining a constant amplitude of 55° . For gait amplitude tests, we evaluated $A = 40^{\circ}$, 55° , and 70° while keeping the spatial frequency fixed at 0.6.

Further, unlike terradynamic environments where quasistatic motion and negligible inertial effects can be assumed, the influence of undulation frequency on locomotion cannot be ignored in aquatic settings. Hence, we conducted experiments to vary the temporal frequency gait parameter. Referring to the gait template Eq. 1, temporal frequency regulates how fast the robot undulates. The experiments tested temporal frequencies from 0.025 Hz to 0.15 Hz in increments of 0.025 Hz. For each temporal frequency value, the robot executed a gait with $G=1,\ A=55^\circ$ and $\xi=0.6$. Frequencies exceeding 0.15 Hz were excluded as the motors were unable to achieve the desired maximum body curvature at such undulation speeds.

C. Experiment protocol

In all robophysical experiments, at the beginning of a trial, the robot was placed into the lattice with a randomly

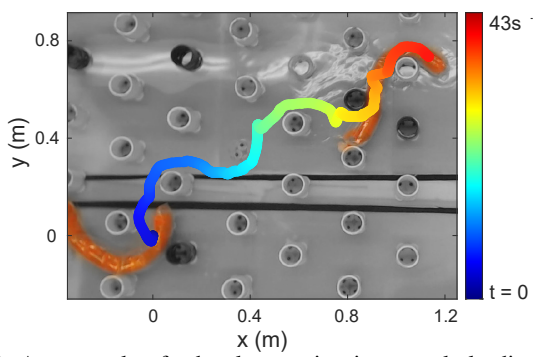


Fig. 3: An example of robot locomotion in a regularly distributed lattice, showing frames of the robot's starting and ending poses, along with its tracked trajectory over time.

selected position and orientation. A trial concluded when the robot either became jammed within the lattice or successfully traversed it. In the results reported in the following section, locomotion performance was evaluated using these key metrics: Distance traveled was computed as the Euclidean distance between the robot's starting and ending positions, while average speed was determined by dividing the distance traveled by the time taken. Success rate was defined as the ratio of experiments in which the robot successfully traversed the lattice to the total number of experiments. Survival rate measured the percentage of experiments in which the robot remained operational (without getting stuck or experiencing motor failure) after traveling a certain distance within the lattice. The trajectories of the robot's body were acquired through overhead video tracking. This tracking process involved affixing a bright dot on the robot's head, and the dot's trajectory was then extracted from videos utilizing the Adobe After Effects motion tracker plugin (Fig. 3).

IV. RESULTS

A. Robophysical experiments

In this section, we present the results of our robophysical experiments. By varying the parameters of generalized compliance (G), gait amplitude (A), spatial frequency (ξ) , and temporal frequency (ω) , we conducted repeated trials with AquaMILR operating under purely feedforward, open-loop control—where the robot executed prescribed undulation motions without sensing-based active adjustments. These experiments enabled us to examine how these parameters influence AquaMILR's behavior and performance within the lattice and to quantify the conditions under which body compliance facilitates spontaneous movement through obstacles.

1) Generalized compliance G: Previous work [1] demonstrated that in the terradynamic regime, the robot exhibited the highest capability to navigate lattices at a mid-range of generalized compliance (G). A small G often led to jamming between obstacles, while a large G resulted in insufficient thrust for forward movement. Jamming occurs when the robot's motion is restricted either by excessive strain from obstacles, exceeding compliance limits and causing immobilization, or by excessive compliance, which prevents the robot from maintaining its undulatory body shape and generating thrust against obstacles. To verify whether this principle

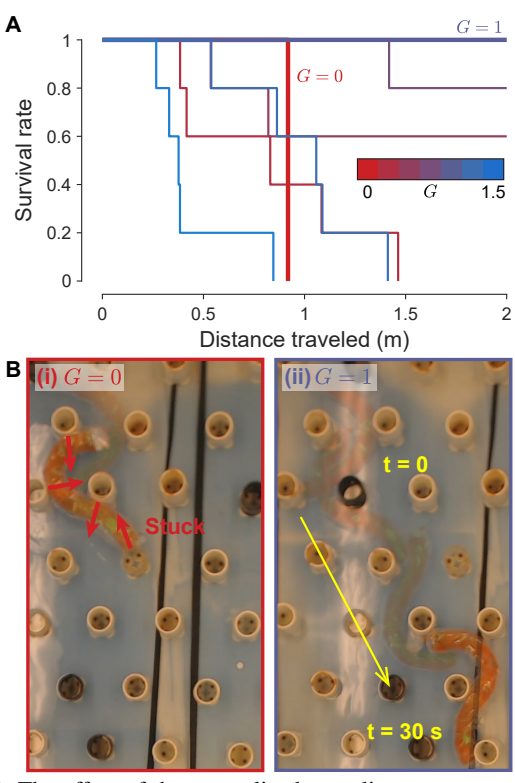


Fig. 4: The effect of the generalized compliance parameter (G) on locomotion performance. (A) The survivor function for varied G values with respect to distance traveled. (B) Time-lapsed frames showing examples of (i) the robot becoming stuck at G=0 and (ii) the robot successfully traversing the lattice at G=1.

extends to the hydrodynamic regime, we experimented with the robot under varied G values, using a fixed gait template that resulted in the same body wavelength-to-post spacing ratio as in the terrestrial case ($A=55^{\circ}, \xi=0.6, \omega=0.05$ Hz). Fig. 4A shows the survival rate as a function of the distance traveled by the robot. The results indicate that a mid-level G remains optimal for navigating obstacles, as reflected by the highest survival rates over distance traveled. Specifically, G = 1 emerged as the most appropriate value, enabling the robot to traverse the lattice in all trials (Fig. 4Bii), demonstrating a manifestation of mechanical intelligence. Our experiments showed that with a low level of G < 0.75, the robot body was too rigid, and when combined with coasting dynamics in the lattice, it often ended up in jamming configurations. At a high level of G > 1, the robot became too compliant, and the inability to maintain the desired body curvature significantly hampered propulsion through the lattice.

2) Gait spatial frequency and amplitude: By varying gait parameters in the template 1, we investigated the robustness of the emergent obstacle navigation over a wide range of gaits. In this set of experiments, we tested the robot with G=0 and G=1, where G=1 was identified previously as the optimal value for successful lattice traversal.

First, we fixed $A=55^\circ$ and varied the spatial frequency. Fig. 5A depicts the successful traverse rate as a function of spatial frequency for both the noncompliant robot (G=0) and the mechanically intelligent robot (G=1). The results

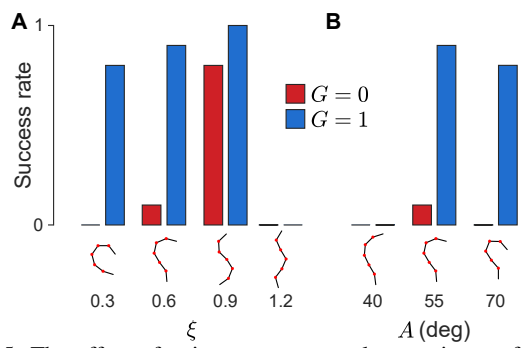


Fig. 5: The effect of gait parameters on locomotion performance. (A) Success traversal rate as a function of spatial frequency (ξ) . (B) Success traversal rate as a function of amplitude (A).

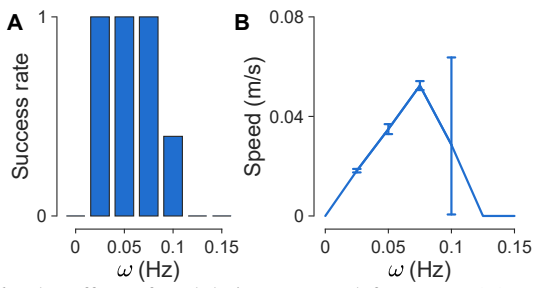


Fig. 6: The effect of undulation temporal frequency (ω) on locomotion performance. (A) Success rate as a function of temporal frequency. (B) Averaged absolute speed of the robot as a function of temporal frequency. Error bars indicate standard deviations.

show that G=1 allows the robot to traverse the lattice over a wider range of spatial frequencies than G=0. Also note that the robot was unable to navigate through spatial frequency values above 0.9, even with G=1. This is likely due to the insufficient curvature in the wave shape, which hinders the robot's ability to latch around obstacles and propel itself forward.

We then fixed $\xi=0.9$ and varied the amplitude. Similar to the results above, Fig. 5B reveals that G=1 allows the robot to traverse the lattice over a wider range of amplitudes than G=0. Overall, although for a specific lattice there is a combination of gait parameters that allows the noncompliant robot to traverse (in this case, $A=55^{\circ}, \xi=0.9$), an appropriate level of body compliance can reduce the sensitivity of robot performance to parameter selection, allowing a wider range of gaits to be effective.

3) Undulation frequency: Previous sections have verified that principles of mechanical intelligence in terrestrial environments can be extended to aquatic environments. However, the largest difference in locomotion between terradynamic and hydrodynamic regimes is the effect of inertia. In the terradynamic regime, locomotion can be assumed quasi-static, making performance insensitive to undulation frequency. Conversely, in the hydrodynamic regime, the coasting effect influences performance with increased undulation frequency leading to increased coasting. Thus, to study the effect of undulation frequency on performance, we varied the temporal frequency (ω) in the gait template Eq. 1, while keeping other parameters fixed ($A=55^{\circ}$, $\xi=0.6$, G=1). Fig. 6 showcases the results for the successful traverse rate and the absolute speed as functions of temporal frequency. The

results first showed a linear relationship in speed from 0.025 Hz to 0.075 Hz, peaking at 0.062 m/s. When $\omega > 0.075$, jamming events started to emerge at $\omega=0.1$ Hz, resulting in a large standard deviation in speed, and became dominant at higher ω . Higher undulation frequency induced more unpredictable collisions, leading to abrupt deviations in the robot's trajectory (as shown in Fig. 3). These collisions increased the probability of jamming instances in the lattice. These findings indicate that at high undulation frequencies in hydrodynamic environments, passive body mechanics alone can no longer effectively mitigate harsh collisions, leading to increased jamming and instability. Consequently, relying solely on mechanical intelligence is insufficient for high-frequency operation and achieving higher absolute speeds in obstaclerich environments. To enhance performance in cluttered fluid settings, computational intelligence—incorporating sensing and decision-making for active adaptation to perturbations must be integrated with mechanical intelligence to improve speed and autonomy.

B. Decentralized body compliance controller development

To enhance robot performance at higher undulation frequencies and in randomly distributed lattices, which better model irregularities often found in natural environments, we developed a feedback controller that can dynamically modulate G in real time based on the torque experienced in the robot joints.

1) Controller design: Instead of using a constant G value for all joints, this controller works in a decentralized manner, i.e., modifies each joint's G locally. The controller modulates the G value of the i-th joint following

$$G_i(\tau) = 1 + 0.2H(\tau_i - 0.3T) + 0.2H(\tau_i - 0.5T) + 0.2H(\tau_i - 0.7T),$$
(4)

where τ_i is the estimated torque experienced in the servo motors that control either the left or the right cable in the i-th joint, and T is the maximum stall torque of the servo motor (1.4 Nm in our case). $H(\cdot)$ represents the step function

$$H(x) = \begin{cases} 0 & x < 0 \\ 1 & x \ge 0 \end{cases} \tag{5}$$

which realizes a three-step torque thresholding mechanism (Fig. 7A). Starting from the most appropriate value G=1, this mechanism allows local G to increase in increments of 0.2. Further, once an increase takes place, the increased G value will be maintained for 0.5 seconds or until the sensed torque drops below the thresholds.

2) Performance test: To test if the controller improved performance, we built a randomly distributed lattice by perturbing the regularly distributed lattice (Fig. 7B). In each experiment, the robot was placed randomly in the lattice with a random orientation, and operated with $\omega=0.15$ Hz. The controller enabled the robot to achieve a 100% successful traverse rate in the random lattice. Fig. 7B and C show an example of a traverse, the G values of all joints and the averaged G values of all joints throughout the entire course, respectively. This example demonstrates that when the robot encounters jamming, even with constant

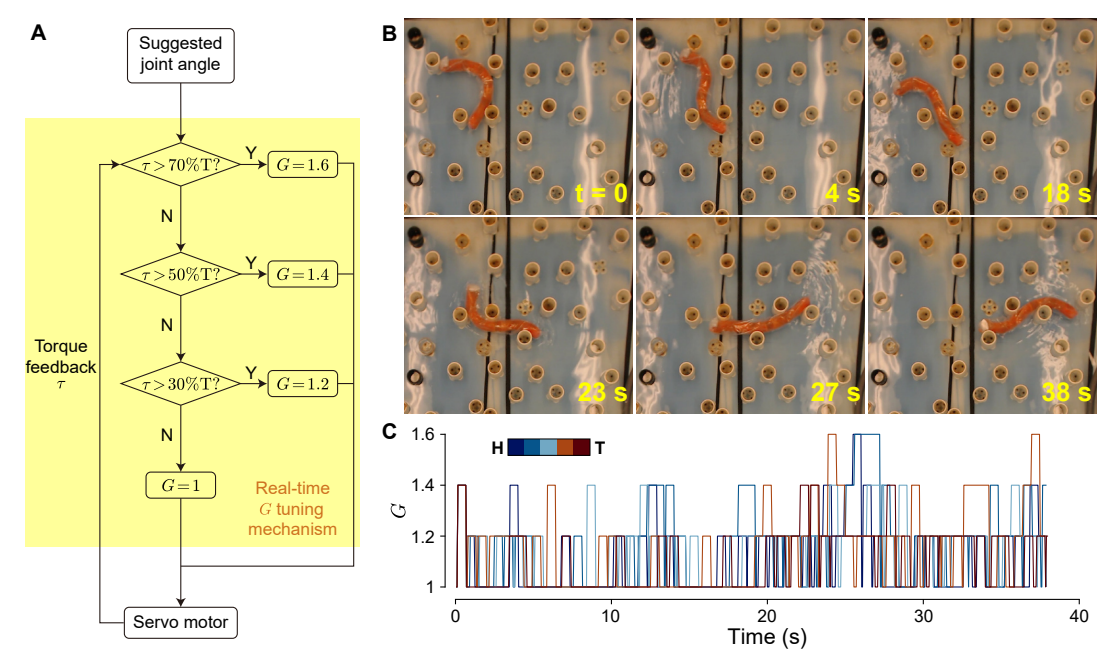


Fig. 7: Computational intelligence enhances mechanical intelligence, improving locomotion capabilities. (A) Block diagram of the decentralized feedback controller implementing real-time local G tuning in each joint. (B) Video snapshots illustrating the robot successfully navigating a challenging, randomly distributed lattice. (C) G values in individual joints over time from head (H) to tail (T) in the example.

body compliance (e.g., t=23 to 27 s), the controller dynamically adjusts compliance, allowing the robot to escape and continue moving. These results highlight that in challenging environments where mechanical intelligence alone is insufficient, computational intelligence provides adaptive control, complementing mechanical intelligence and further enhancing the robot's locomotion capabilities.

3) Discussion: In addition to enhancing performance, we observed during experiments that this control mechanism allowed the robot to function as a sensing tool to probe the density of its surrounding environment. For example, from t = 23 to 27 s, where we observed an emergent increase in G (Fig. 7C), indicating an increasing obstacle density around the robot. We can also roughly estimate which portion of the body experiences peak environmental forces, due to the decentralized nature of the controller. Studies have shown the importance of not only navigating unknown environments but also having the ability to characterize surroundings [34], [35]. Knowledge of the environment can lead to better-informed decisions for locomotion strategies on hazardous or challenging terrain. Thus, we hypothesize that, when coupled with an on-board localization and mapping system, AquaMILR with the real-time G tuning mechanism can be used to probe heterogeneous aquatic environments while locomoting within them.

Video clips of robot experiments can be found in SI movie: https://youtu.be/K7s5Wt3Qs14.

V. CONCLUSION

In this work, we developed an untethered limbless robot, AquaMILR, that extends the bilateral actuation mechanism, programmable body compliance, and the principles of limbless mechanical intelligence to the hydrodynamic regime. Through a series of robophysical experiments, we confirmed that while these principles generally hold, the effectiveness of passive body compliance is constrained by undulation frequency due to the influence of inertial effects in hydrodynamic environments, which play a more significant role than in terradynamic settings. Further, we developed a decentralized feedback controller that can modulate local body compliance in real time, allowing the robot to navigate through disordered heterogeneous aquatic environments at high undulation frequencies. Our results demonstrate that computational intelligence can complement mechanical intelligence, improving the robustness of locomotion.

This work paves the way for the future development of bilaterally actuated limbless robots for swimming in heterogeneous environments. Future work includes the development of onboard sensing modalities for sophisticated controller design, upgrades to enable the robot to follow a path at various depths and access 3D heterogeneous environments freely [36], and the development of amphibious robots that can transition between multiple locomotion modes, such as lateral undulation and sidewinding [37], on/in varied substrates. Further, based on this case study, we aim to further understand and model the synergy between mechanical intelligence and computational intelligence in hydrodynamic settings, which could potentially improve the locomotion efficacy and efficiency of underwater limbless robots.

VI. ACKNOWLEDGEMENT

The authors would like to thank Bangyuan Liu and Frank L. Hammond III for providing preliminary test environment and apparatus; Anushka Bhumkar for helping with robot maintenance and experiments; Christopher J. Pierce for useful discussions. This study is supported by Army Research Office grant (W911NF-11-1-0514) and NSF Physics of Living Systems Student Research Network (GR10003305).

REFERENCES

- T. Wang, C. Pierce, V. Kojouharov, B. Chong, K. Diaz, H. Lu, and D. I. Goldman, "Mechanical intelligence simplifies control in terrestrial limbless locomotion," *Science Robotics*, vol. 8, no. 85, p. eadi2243, 2023.
- [2] R. K. Katzschmann, J. DelPreto, R. MacCurdy, and D. Rus, "Exploration of underwater life with an acoustically controlled soft robotic fish," *Science Robotics*, vol. 3, no. 16, p. eaar3449, 2018.
- [3] J. Zhu, C. White, D. K. Wainwright, V. Di Santo, G. V. Lauder, and H. Bart-Smith, "Tuna robotics: A high-frequency experimental platform exploring the performance space of swimming fishes," *Science Robotics*, vol. 4, no. 34, p. eaax4615, 2019.
- [4] R. Thandiackal, K. Melo, L. Paez, J. Herault, T. Kano, K. Akiyama, F. Boyer, D. Ryczko, A. Ishiguro, and A. J. Ijspeert, "Emergence of robust self-organized undulatory swimming based on local hydrodynamic force sensing," *Science robotics*, vol. 6, no. 57, p. eabf6354, 2021.
- [5] R. Baines, S. K. Patiballa, J. Booth, L. Ramirez, T. Sipple, A. Garcia, F. Fish, and R. Kramer-Bottiglio, "Multi-environment robotic transitions through adaptive morphogenesis," *Nature*, vol. 610, no. 7931, pp. 283–289, 2022.
- [6] T. Wang, H.-J. Joo, S. Song, W. Hu, C. Keplinger, and M. Sitti, "A versatile jellyfish-like robotic platform for effective underwater propulsion and manipulation," *Science Advances*, vol. 9, no. 15, p. eadg0292, 2023.
- [7] K. Ren and J. Yu, "Research status of bionic amphibious robots: A review," *Ocean Engineering*, vol. 227, p. 108862, 2021.
- [8] J. Lin, Z. Guo, and A. Badri-Spröwitz, "Bird-inspired tendon coupling improves paddling efficiency by shortening phase transition times," arXiv preprint arXiv:2409.14707, 2024.
- [9] W.-S. Chu, K.-T. Lee, S.-H. Song, M.-W. Han, J.-Y. Lee, H.-S. Kim, M.-S. Kim, Y.-J. Park, K.-J. Cho, and S.-H. Ahn, "Review of biomimetic underwater robots using smart actuators," *International journal of precision engineering and manufacturing*, vol. 13, pp. 1281–1292, 2012.
- [10] A. Raj and A. Thakur, "Fish-inspired robots: design, sensing, actuation, and autonomy—a review of research," *Bioinspiration & biomimetics*, vol. 11, no. 3, p. 031001, 2016.
- [11] R. Wang, S. Wang, Y. Wang, L. Cheng, and M. Tan, "Development and motion control of biomimetic underwater robots: A survey," *IEEE Transactions on Systems, Man, and Cybernetics: Systems*, vol. 52, no. 2, pp. 833–844, 2020.
- [12] J. Qu, Y. Xu, Z. Li, Z. Yu, B. Mao, Y. Wang, Z. Wang, Q. Fan, X. Qian, M. Zhang et al., "Recent advances on underwater soft robots," Advanced Intelligent Systems, vol. 6, no. 2, p. 2300299, 2024.
- [13] R. Bogue, "Underwater robots: a review of technologies and applications," *Industrial Robot: An International Journal*, vol. 42, no. 3, pp. 186–191, 2015.
- [14] G. Li, G. Liu, D. Leng, X. Fang, G. Li, and W. Wang, "Underwater undulating propulsion biomimetic robots: A review," *Biomimetics*, vol. 8, no. 3, p. 318, 2023.
- [15] A. Crespi and A. J. Ijspeert, "Online optimization of swimming and crawling in an amphibious snake robot," *IEEE Transactions on robotics*, vol. 24, no. 1, pp. 75–87, 2008.
- [16] P. Liljebäck, Ø. Stavdahl, K. Y. Pettersen, and J. T. Gravdahl, "Mambaa waterproof snake robot with tactile sensing," in 2014 IEEE/RSJ International Conference on Intelligent Robots and Systems. IEEE, 2014, pp. 294–301.
- [17] Z. Zuo, Z. Wang, B. Li, and S. Ma, "Serpentine locomotion of a snake-like robot in water environment," in 2008 IEEE International Conference on Robotics and Biomimetics. IEEE, 2009, pp. 25–30.
- [18] H. Yamada, S. Chigisaki, M. Mori, K. Takita, K. Ogami, and S. Hirose, "Development of amphibious snake-like robot acm-r5, isr2005," *Proceedings of ISR*, p. 133, 2005.
- [19] F. Sanfilippo, J. Azpiazu, G. Marafioti, A. A. Transeth, Ø. Stavdahl, and P. Liljebäck, "Perception-driven obstacle-aided locomotion for snake robots: the state of the art, challenges and possibilities," *Applied Sciences*, vol. 7, no. 4, p. 336, 2017.
- [20] E. Kelasidi, S. Moe, K. Y. Pettersen, A. M. Kohl, P. Liljebäck, and J. T. Gravdahl, "Path following, obstacle detection and obstacle avoidance for thrusted underwater snake robots," *Frontiers in Robotics and AI*, vol. 6, p. 57, 2019.

- [21] A. A. Transeth, R. I. Leine, C. Glocker, K. Y. Pettersen, and P. Liljebäck, "Snake robot obstacle-aided locomotion: Modeling, simulations, and experiments," *IEEE Transactions on Robotics*, vol. 24, no. 1, pp. 88–104, 2008.
- [22] B. Chong, T. Wang, D. Irvine, V. Kojouharov, B. Lin, H. Choset, D. I. Goldman, and G. Blekherman, "Gait design for limbless obstacle aided locomotion using geometric mechanics," in *Robotics: science* and systems, 2023.
- [23] T. Wang, J. Whitman, M. Travers, and H. Choset, "Directional compliance in obstacle-aided navigation for snake robots," in 2020 American Control Conference (ACC), 2020, pp. 2458–2463.
- [24] D. Ramesh, Q. Fu, and C. Li, "Sensnake: A snake robot with contact force sensing for studying locomotion in complex 3-d terrain," in 2022 International Conference on Robotics and Automation (ICRA). IEEE, 2022, pp. 2068–2075.
- [25] Q. Fu and C. Li, "Robotic modelling of snake traversing large, smooth obstacles reveals stability benefits of body compliance," *Royal Society* open science, vol. 7, no. 2, p. 191192, 2020.
- [26] J. H. Boyle, S. Johnson, and A. A. Dehghani-Sanij, "Adaptive undulatory locomotion of a c. elegans inspired robot," *IEEE/ASME Transactions on Mechatronics*, vol. 18, no. 2, pp. 439–448, 2012.
- [27] B. Liu and F. L. Hammond, "Nonbiomorphic passively adaptive swimming robot enables agile propulsion in cluttered aquatic environments," Soft Robotics, vol. 10, no. 5, pp. 884–896, 2023.
- [28] J. Carling, T. L. Williams, and G. Bowtell, "Self-propelled anguilliform swimming: simultaneous solution of the two-dimensional navier–stokes equations and newton's laws of motion," *Journal of experimental biology*, vol. 201, no. 23, pp. 3143–3166, 1998.
- [29] M. Gazzola, M. Argentina, and L. Mahadevan, "Gait and speed selection in slender inertial swimmers," *Proceedings of the National Academy of Sciences*, vol. 112, no. 13, pp. 3874–3879, 2015.
- [30] N. Justus and R. Hatton, "Optimal gaits for inertia-dominated swimmers with passive elastic joints," *Physical Review E*, vol. 109, no. 3, p. 034602, 2024.
- [31] J. M. Rieser, B. Chong, C. Gong, H. C. Astley, P. E. Schiebel, K. Diaz, C. J. Pierce, H. Lu, R. L. Hatton, H. Choset *et al.*, "Geometric phase predicts locomotion performance in undulating living systems across scales," *Proceedings of the National Academy of Sciences*, vol. 121, no. 24, p. e2320517121, 2024.
- [32] J. Aguilar, T. Zhang, F. Qian, M. Kingsbury, B. McInroe, N. Mazouchova, C. Li, R. Maladen, C. Gong, M. Travers et al., "A review on locomotion robophysics: the study of movement at the intersection of robotics, soft matter and dynamical systems," *Reports on Progress in Physics*, vol. 79, no. 11, p. 110001, 2016.
- [33] S. Hirose, "Biologically inspired robots," Snake-Like Locomotors and Manipulators, 1993.
- [34] F. Qian, D. Lee, G. Nikolich, D. Koditschek, and D. Jerolmack, "Rapid in situ characterization of soil erodibility with a field deployable robot," *Journal of Geophysical Research: Earth Surface*, vol. 124, no. 5, pp. 1261–1280, 2019.
- [35] J. Bush, Y. Zhang, S. Liu, E. Fulcher, C. Franklin, D. Jerolmack, R. Ewing, K. Fisher, and F. Qian, "Robotic legs as novel planetary instrumentation to explore the mechanical properties of regolith," *LPI Contributions*, vol. 2806, p. 1733, 2023.
- [36] M. Fernandez, T. Wang, G. Tunnicliffe, D. Dortilus, P. Gunnarson, J. O. Dabiri, and D. I. Goldman, "Aquamilr+: Design of an untethered limbless robot for complex aquatic terrain navigation," arXiv preprint arXiv:2409.18383, 2024.
- [37] V. Kojouharov, T. Wang, M. Fernandez, J. Maeng, and D. I. Gold-man, "Anisotropic body compliance facilitates robotic sidewinding in complex environments," in 2024 International Conference on Robotics and Automation (ICRA). IEEE, 2024.